Dynamic modelling of wind farm grid interaction

Anca D. Hansen[1], Poul Sørensen[1], Frede Blaabjerg[2] and John Becho[3]
1 Risø National Laboratory, Wind Energy Department, DK-4000 Roskilde, Denmark; emails <anca.daniela.hansen@risoe.dk>, <poul.soerensen@risoe.dk>
2 Aalborg University, Pontoppidanstræde 101, P.O. Box 49, 9220 Aalborg East, Denmark, DK; email < fbl@iet.auc.dk>
3 NEG-Micon Control Systems, Italiensvej 1-5, DK-8450 Hammel; email < jbe@dancontrol-eng.dk>

ABSTRACT

This paper describes a dynamic model of a wind farm and its nearest utility grid. It is intended to use this model in studies addressing the dynamic interaction between a wind farm and a power system, both during normal operation of the wind farm and during transient grid fault events. The model comprises the substation where the wind farm is connected, the internal power collection system of the wind farm, the electrical, mechanical and aerodynamic models for the wind turbines, and a wind model. The integrated model is built to enable the assessment of power quality and control strategies. It is implemented in the commercial dedicated power system simulation tool DIgSILENT.

1 INTRODUCTION

The motivation for this investigation is the ever-increasing wind energy penetration into power networks. In recent years the trend has been moved from installations with a few wind turbines to the planning of large wind farms with more than hundreds of MW of capacity. This increased and concentrated penetration makes the power network more dependent on, and vulnerable to, the wind energy production. This situation means that future wind farms must be able to replace conventional power stations, and thus be active controllable elements in the power supply network. In other words, wind farms must develop power plant characteristics (Sørensen P. et al., 2000). The two utilities responsible in Denmark for power supply networks, Eltra and Elkraft System, have issued requirements (Eltra, 2000) that focus on the influence of wind farms on grid stability and power quality, and on the control capabilities of wind farms.

Another consequence of the increased future size of wind farms is that the large wind farms will be connected directly to the high voltage transmission grid. Until now, wind turbines and wind farms have been connected to the distribution system, which typically has either 10/ 20 kV or 50/ 60 kV grids. Therefore, the main focus has been on the influence of the wind farms on the power quality of the distribution system. For example in Denmark, this has been regulated by the Danish Utilities Research Institute (DEFU) requirements for grid connection of wind turbines to the distribution system (DEFU KR111, 1998). However, the transmission system operators in Denmark now issue more strict connection requirements for large wind farms if they are connected directly to the transmission system. Moreover, national standards for power quality of wind turbines have recently been supplemented by a new standard for measurement and assessment of power quality of grid connected wind turbines, namely (IEC 61400-21, 2001).

Having in mind all these aspects, it is important to appreciate the information provided by models that simulate the dynamic interaction between a wind farm and a power system. Such

developed models enable both the wind farm investors and the utility grid technical staff, to perform the necessary preliminary studies before connecting wind farms to the grid. Simulation of the wind farm interaction with the grid may thus provide valuable information and may even lower the overall grid connection costs. The present work describes the first steps to provide such models. The described wind farm simulation model is the first of its kind and represents a complex tool in the prediction of the influence of wind farms on the power quality. The model can be used and even further extended in order to study different aspects related to the connection of the wind farms to the grid, i.e. control strategies, connection to weak grids, HVDC connections and storage systems.

This paper presents the main result of a national Danish research project, namely a wind farm model capable of simulating the interaction between a wind farm and its power network, both during normal operation and during transient grid fault events (Sørensen P. et al., 2001a). The model is developed in the power system simulation tool DIgSILENT, which provides both an extensive library for grid components and a dynamic simulation language (DSL) for the modelling of each wind turbine component. The case study for this research is the 12 MW wind farm installed in Hagesholm, Denmark, which consists of six NM-2000 constant speed wind turbines from NEG-Micon, each of 2 MW rated power with active stall control. Hagesholm wind farm is connected to a strong grid compared to the wind farm power capacity. This small-scale case study establishes the first steps toward the large-scale case study, i.e. a 150 MW wind farm connected to the transmission network.

The whole wind farm model comprises a grid model, six almost identical wind turbine models and a wind speed model, as follows:

- *the grid model* includes the electric components in the wind farm power collection system and the substation, and uses equivalents for the remaining grid.
- *the individual wind turbine model* includes electrical, mechanical and aerodynamic submodels:
  - the electrical submodel consists of an induction generator, a soft-starter, a capacitor bank for reactive power compensation and a step-up transformer.
  - the mechanical submodel describes the dynamics of the drive train.
  - the aerodynamic submodel is a standard C_p based model, extended with dynamic stall effects.
- *the wind speed model* outputs the wind speeds for each wind turbine in the wind farm, taking into account the coherence and the effects of wind variations in the rotor plane (e.g. 3p fluctuations due to rotationally sampled turbulence and tower shadow of the 3-bladed turbine).

The simulation model is validated in the first place, for fault-free operation, based on power quality measurement data on a wind turbine from Hagesholm wind farm, and the results are promising.

2 MODELLING TOOL

Computer models of power systems are widely used by power system utilities to study load flow, steady state voltage stability and dynamic behaviour of power systems. The models presented in this paper are implemented in the power system simulation tool DIgSILENT, because it provides the ability to simulate load flow, RMS fluctuations and transient events in the same software environment.

DIgSILENT provides a comprehensive library of models for electrical components in the

power system e.g. generators, motors, power plant controllers, dynamic loads and various passive network elements, such as lines, transformers, static loads and shunts. In the present work, the grid model and the electrical components of the wind turbine are built with standard component models from the DIgSILENT library. The models of the wind speed, of the mechanical, of the aerodynamic and control parts of the wind turbines, are implemented in the dynamic simulation language DSL of DIgSILENT. DSL allows the user to implement specific models that are not standard in DIgSILENT library, and thus to create own developed blocks, either as modifications of existing models or as completely new models. These developed models are gathered in a personal library, which can be used easily for further modelling of other wind farms with different wind turbines.

DIgSILENT provides models with different detailing levels in a very well structured way. It combines the traditional transient EMT (electromagnetic transient) simulation tool for power systems with RMS simulations of longer-term dynamics. Depending on the goal of the analysis, it is possible to select the appropriate detailed models, by choosing the type of simulation method. The RMS simulations are based on electromechanical transient models, which are more simplified models than the electromagnetic transient models used in EMT simulations. RMS simulations are more appropriate for long simulation periods without transients, as in most studies of power quality and control issues. On the other hand, simulations of instantaneous EMT values with detailed models are required for reliable simulations of the behaviour during grid faults.

3 GRID MODELLING

Hagesholm wind farm consists of six NM 2000/72 turbines from NEG-Micon, each of 2 MW rated power with active stall control. The wind farm is connected via two feeders to the 10 kV busbar in 50/10kV substation in Grevinge, which is located 5 km away from the wind farm.

The network layout of Hagesholm wind farm is sketched in Figure 1. It illustrates how these six wind turbines are distributed in two groups in their connection to the substation. Each of the 6 wind turbines WT1, WT2,.., WT6 are connected to its own 10kV terminals called "WT1_10kV",.., "WT6_10kV", respectively. Each terminal represents the wind turbine terminal to the grid. A backup line, normally disconnected, is also installed between the ends of the two lines. Two identical 16MVA 50/10kV transformers are installed in Grevinge substation, of which only one (TR1-50/10kV in Figure 1) is connected in normal operation conditions. The other transformer (disconnected) serves as a backup.

Both the connection of the wind farm to the substation and the substation itself are modelled by the actual physical components (transformers, line, load, busbar), while a simplified equivalent Thevenin is used to model the remaining power system (50 kV grid). This is a fair approximation for power quality studies, as the grid is very strong compared to the power capacity of the whole wind farm.

The load feeders, which are also connected to the Grevinge substation, are modelled in the first place as a single, general load connected to the substation directly to the 10kV busbar of the substation – see Figure 1.

4 WIND TURBINE MODELLING

The wind turbine model includes electrical, mechanical and aerodynamic models (Sørensen P. et al., 2001a). Each of the six wind turbines of Hagesholm wind farm has its own model, which enables simulation of the interaction between the wind turbines in the wind farm. The model also makes it possible to simulate with different generator types on the individual wind

turbines, as it is the case in Hagesholm. Besides of different generator parameters, the wind turbine models are identical.

Figure 2 illustrates the overall structure of the wind turbine model. It consists of an aerodynamic, a mechanical and an electrical model, with an overall control system model. The wind model provides an equivalent wind speed v_{eq} as input to the aerodynamic model. The equivalent wind speed v_{eq} (see Section 5) takes into account the rotational turbulence, the tower shadow and the variations in the whole wind speed field over the rotor disk, by using the information from the mechanical system about the turbine rotor position θ_{wtr}. Besides the equivalent wind speed veq, the pitch angle θ_{pitch} from the control system and the wind turbine rotor speed ω_{wtr} from the mechanical model constitute the inputs of the aerodynamic model. The output of the aerodynamic model is the aerodynamic torque T_{ae}, which is input for the mechanical model together with the generator speed ω_{gen}. The mechanical model delivers the mechanical turbine power P_t to the generatowr model. The electrical model interfaces with the power system by the voltages U_{wtt} and currents I_{wtt} on the (10 kV) wind turbine terminals. The control system uses as inputs the following signals: 1) the hub wind speed v_{hub} (fixed-point wind speed), 2) the generator speed ω_{gen} and, 3) the active power P_{ms} and reactive power Q_{ms} at the main switch, representing the measured voltages and currents of the control system. The control system has as outputs: 1) the pitch angle θ_{pitch} to the aerodynamic model, 2) the soft-starter angle α_{ss} and, 3) the capacitor bank switch signals S_C to the electrical model.

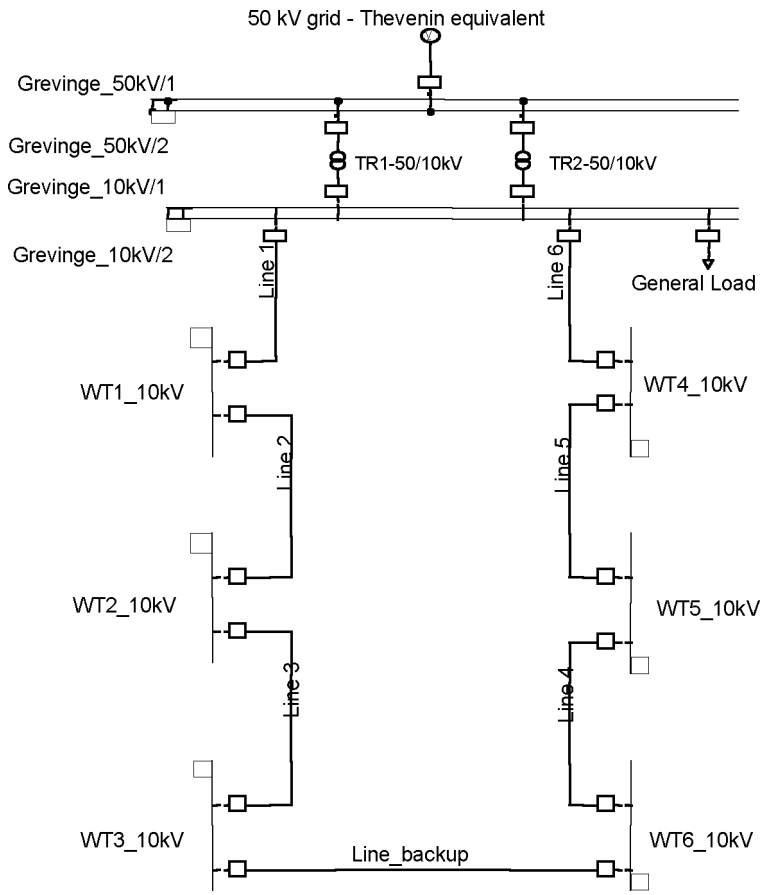

Figure 1 Single line diagram of the Hagesholm wind farm grid in DIgSILENT

4.1 Aerodynamic model

Standard aerodynamic programs typically use blade element methods and therefore they require considerable computation time. This is not adequate to simulate a wind farm with several wind turbines. Therefore the present aerodynamic model is based on the aerodynamic efficiency $C_p(\lambda,\theta_{pitch})$, which is calculated by a standard aerodynamic program. This simplification is acceptable as long as only the effect on the power, namely the aerodynamic torque T_{ae}, is taken into account.

For a given rotor, $C_p(\lambda,\theta_{pitch})$ depends on the pitch angle θ_{pitch} and on the tip speed ratio $\lambda = R\omega_{wtr}/v_{eq}$. The aerodynamic efficiency, usually tabled as a matrix in the aerodynamic program, is used to determine the quasi static aerodynamic power P_{ae} developed on the main shaft of a wind turbine with rotor radius R at a wind speed v_{eq} and air density ρ:

$$P_{ae} = \tfrac{1}{2}\rho\pi R^2 v_{eq}^{\ 3} C_p(\theta_{pitch},\lambda) \tag{1}$$

Once the aerodynamic power is determined, the aerodynamic torque T_{ae} can be calculated directly according to:

$$T_{ae} = \frac{P_{ae}}{\omega_{wtr}} = \frac{\pi}{2\lambda}\rho R^3 v_{eq}^{\ 2} C_p(\theta_{pitch},\lambda) \tag{2}$$

The simplification of using a steady state aerodynamic efficiency, instead of a dynamic aerodynamic efficiency, in Equation (1) corresponds to the steady state aero loads. This simplification underestimates the actual power fluctuations in the stall region. For the sake of simplicity, from now on, the steady state aerodynamic efficiency is denoted by C_p^{static}, while the dynamic aerodynamic efficiency is referred by $C_p^{dynamic}$. Figure 3 illustrates the power curve of a wind turbine and how large the power fluctuations are, as caused by wind speed fluctuations for two situations: low wind speed region ($u < 8$ m/s – case 1) and high wind speed region ($u > 8$ m/s – case 2). For low wind speeds (case 1) there is no significant difference between the static power P^{static} and the dynamic power $P^{dynamic}$, because the amplification factors of the fluctuations for both steady state and dynamic state are similar. This is not the case for the high wind speeds (case 2) in the stall region, where, due to the dynamic stall effects, fluctuations in wind speed, produce larger power fluctuations.

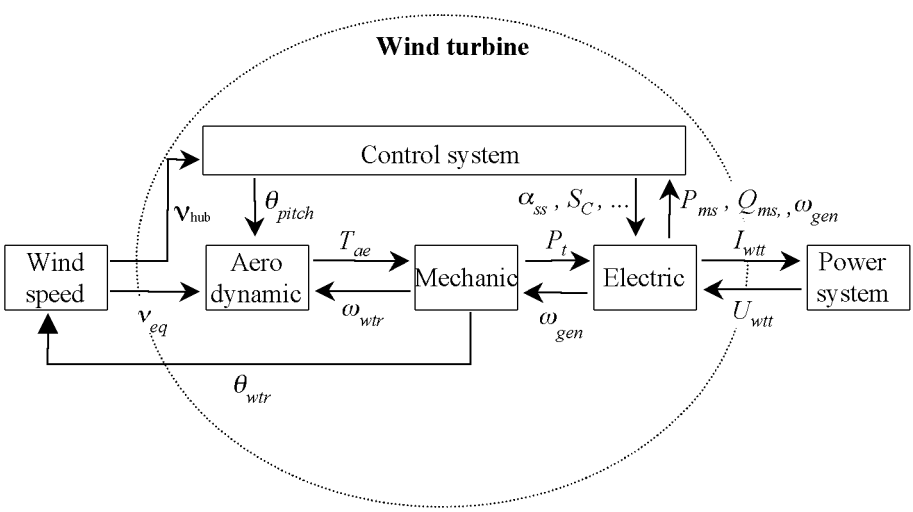

Figure 2 General structure of the wind turbine model

The DIgSILENT aerodynamic model is improved with a model for the dynamic stall effects. The applied model for the dynamic stall is an enhancement of the method described in (Øye & S., 1991). This former method simulates the dynamic stall as time lag of separation and it implements the time lag directly on the lift coefficients. The present aerodynamic model, implemented in DIgSILENT, is based on the aerodynamic efficiency coefficient C_p, instead of the lift coefficients C_L. The dynamic aerodynamic efficiency, $C_p^{dynamic}$, is determined as based on the static aerodynamic efficiency, C_p^{static}, and two additional aerodynamic efficiencies concerning the wind profile around the wing, i.e. one for attached flow and the other for separated flow. The attached flow corresponds to the steady state flow at low angles of attack, while the separated flow corresponds to the steady state flow at high angles of attack (Øye & S., 1991). Thus, for a certain pitch angle, θ_{pitch}, and tip speed ratio, λ, the three aerodynamic coefficient tables provide respectively the values for $C_p^{attached}$, C_p^{static} and $C_p^{separated}$. The static value of the separation ratio f_{st} is computed as illustrated in Figure 4. Then, the dynamic separation ratio f is obtained by using a low pass filter, with the time constant (lag) approximated by $\tau = 4/u_0$, where u_0 is the mean wind speed.

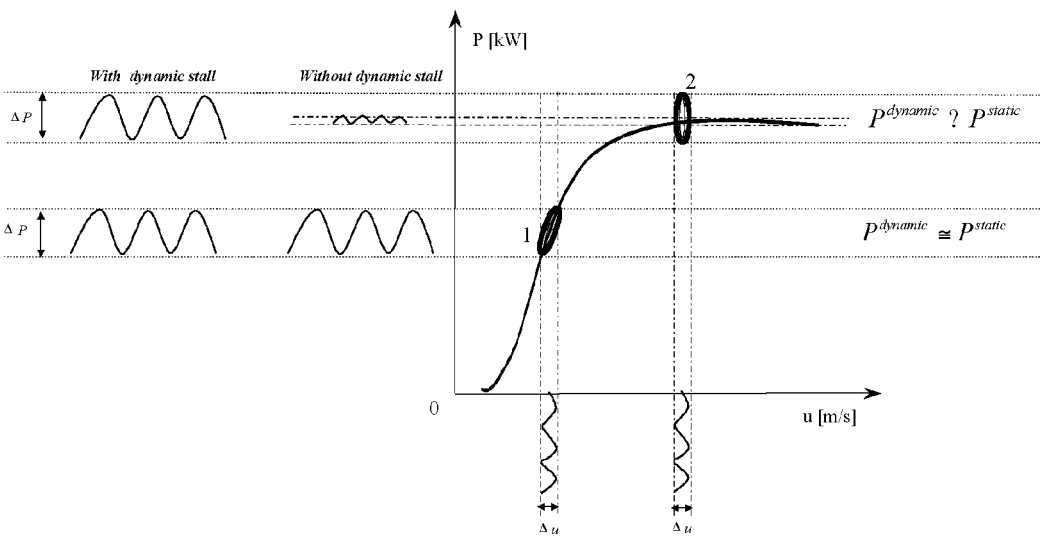

Figure 3 Power fluctuations in the stall region with and without dynamic stall

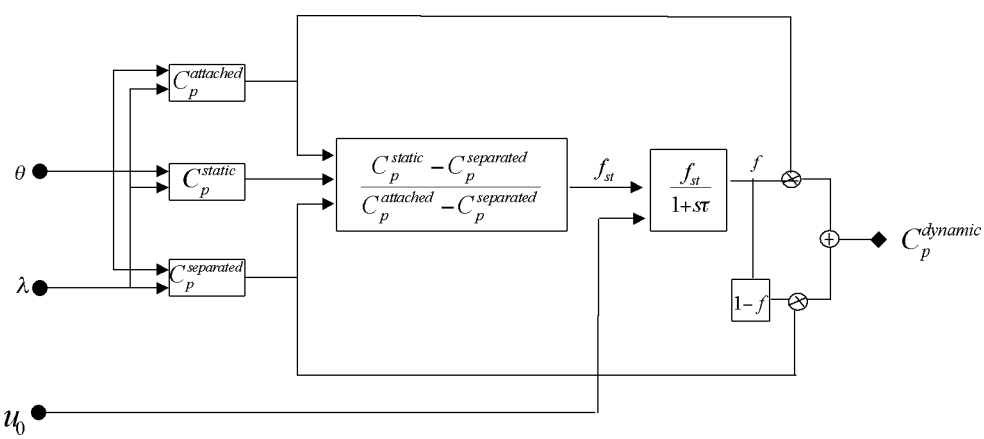

Figure 4 DIgSILENT block diagram for dynamic stall

Finally, the dynamic value of the aerodynamic coefficient is determined through the interpolation:

$$C_p^{dynamic} = f\, C_p^{attached} + (1-f)\, C_p^{separated} \tag{3}$$

This value is then used in the aerodynamic power expression (1) to estimate the power fluctuations in the stall region.

4.2 Mechanical model

In the mechanical model, Figure 5, emphasis is put only on those parts of the dynamic structure of the wind turbine that contribute to the interaction with the grid. Therefore only the drive train is considered in the first place, because this part of the wind turbine has the most significant influence on the power fluctuations. The other parts of the wind turbine structure, e.g. tower and the flap bending modes, are thus neglected.

The drive train converts the aerodynamic torque T_{ae} on the rotor into the torque on the low speed shaft T_{lss}, which is scaled down through the gearbox to the torque on the high-speed shaft T_{hss}. The drive train model is a typical 2-mass model, connected by a flexible low speed shaft, which is modelled by a stiffness k_s and damping coefficient c_s. The masses used in the model correspond to large turbine rotor inertia I_{wtr}, representing the blades and the hub, and a small inertia I_{gen} representing the induction generator. Moreover, an ideal gear with the exchange ratio (1:η) is included in the model. The high-speed shaft is assumed to be stiff: $T_{hss} = T_{lss} / \eta$.

The generator's inertia I_{gen} is implemented in DIgSILENT as a part of the generator model, while the remaining part of the mechanical model is described in a state space form in the dynamic simulation language DSL of DIgSILENT. The input variables $\bar{u}$, the output variables $\bar{y}$ and the state variables $\bar{x}$, respectively, are defined as follows:

$$\bar{u} = \begin{pmatrix} \omega_{gen} \\ T_{ae} \end{pmatrix}, \; \bar{y} = \begin{pmatrix} T_{hss} \\ \theta_{wtr} \\ \omega_{wtr} \end{pmatrix}, \; \bar{x} = \begin{pmatrix} \theta_k \\ \theta_{wtr} \\ \omega_{wt} \end{pmatrix} \tag{4}$$

where θ_k is the angular difference between the two ends of the flexible shaft, i.e.

$$\theta_k = \theta_{wtr} - \theta_{lss} = \theta_{wtr} - \frac{\theta_{gen}}{\eta} \tag{5}$$

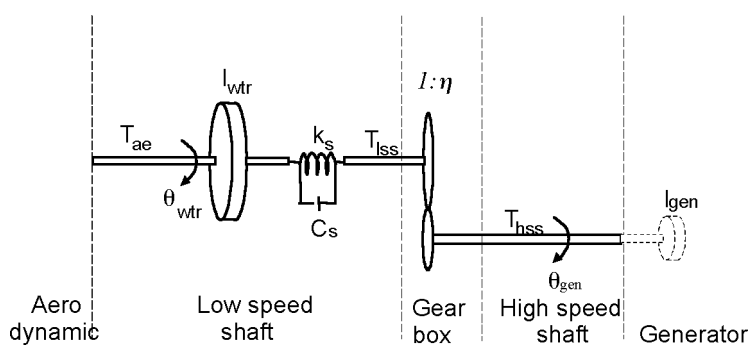

Figure 5 Drive train model

The state space equations of the mechanical model are then:

$$\dot{\bar{x}} = \begin{pmatrix} 0 & 0 & 1 \\ 0 & 0 & 1 \\ \frac{-k_s}{I_{wtr}} & 0 & \frac{-c_s}{I_{wtr}} \end{pmatrix} \cdot \bar{x} + \begin{pmatrix} -\frac{1}{\eta} & 0 \\ 0 & 0 \\ \frac{c_s}{\eta \cdot I_{wtr}} & \frac{1}{I_{wtr}} \end{pmatrix} \cdot \bar{u} \tag{6}$$

$$\bar{y} = \begin{pmatrix} \frac{k_s}{\eta} & 0 & \frac{c_s}{\eta} \\ 0 & 1 & 0 \\ 0 & 0 & 1 \end{pmatrix} \cdot \bar{x} + \begin{pmatrix} -\frac{c_s}{\eta^2} & 0 \\ 0 & 0 \\ 0 & 0 \end{pmatrix} \cdot \bar{u} \tag{7}$$

The damping coefficient c_s is given by:

$$c_s = 2\,\xi\,\sqrt{k_s\,I_{wtr}} \tag{8}$$

where ξ is the damping ratio and can be expressed using the logarithmic decrement δ_s:

$$\xi = \frac{\delta_s}{\sqrt{\delta_s^2 + 4\pi^2}} \tag{9}$$

The logarithmic decrement is the logarithm of the ratio between the amplitude at the beginning of the period and the amplitude at the end of the next period of the oscillation:

$$\delta_s = 1\mathrm{n}\left(\frac{a(t)}{a(t+tp)}\right) \tag{10}$$

where α denotes the amplitude of the signal.

4.3 Electrical model

The electric design of each wind turbine in Hagesholm is based on the typical "Danish" concept, with two induction generators, a soft-starter, capacitor banks for power factor compensation and a step-up transformer – see Figure 6.

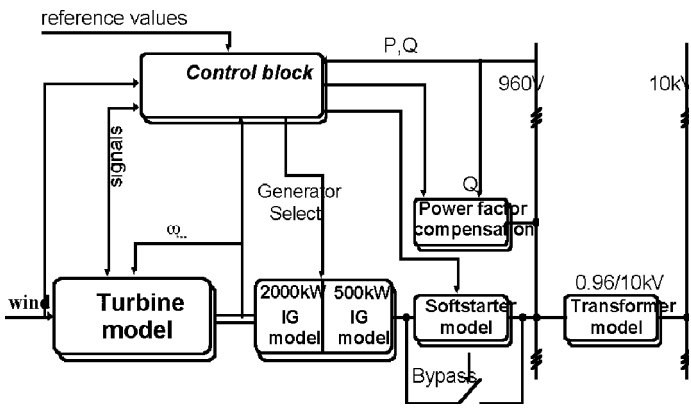

Figure 6 Simplified electrical scheme a wind turbine

Only one generator is connected to the 960V busbar, at a time. This corresponds to the two sets of windings in the real generator that may operate with 4 or 6 poles.

DIgSILENT provides models as modules for the electrical components of the wind turbine, namely generator, soft-starter, capacitor banks for reactive power compensation, transformer, tower cable and busbar. The control system is implemented in DIgSILENT dynamic simulation language DSL.

The electrical part of the wind turbine WT1, implemented in DIgSILENT, is illustrated in Figure 7. It contains all the electrical components of the wind turbine from the tower bottom to the nacelle in the tower top. The 10kV terminal of the first wind turbine "WT1_10kV" is identical to the terminal with the same name in Figure 1. The scheme presented in Figure 7 is "an extension" of the single line diagram, shown in Figure 1. The scheme focuses on the electrical model of the wind turbine. Terminals "WT1_10kV" and "WT1_Top_10kV" correspond physically to the bottom and to the top of the wind turbine, respectively. The 960 V busbar, with main switch MSP, the capacitor bank (C1_t1,..C10_t1) and the soft-starter are placed in the nacelle. As the LV/MV step-up transformer "2-Winding Transformer_t1" is also placed in the nacelle, the "Tower Cable_t1" is a medium voltage MV cable. The generator in the NM-2000 wind turbine is a squirrel cage induction type. Besides the electro-magnetic description, the generator model in DIgSILENT also contains the mechanical inertia of the generator rotor, as it was mentioned in the previous section.

The cut-in of the generator to the grid is performed by a soft-starter using firing angle control, when the generator speed reaches the synchronous speed. When the soft-starter is bypassed, and thus the generator is connected, the power factor compensation is performed by the capacitor bank. The capacitor bank consists of 10 capacitors controlled independently.

Based on the reactive power Q_{ms}, measured on the low voltage side of the step-up transformer at the main switch point MSP, the control system close or open the individual capacitors C1_t1,.., C10_t, Figure 7. Figure 8 illustrates the DIgSILENT block diagram for the capacitor bank controller. The diagram is general for the simulation of capacitor bank switchings, and consequently it can also be used to simulate other wind turbines. Only the number of steps and averaging time may differ from one wind turbine type to another.

The switching of capacitors is done based on the average value of the measured reactive power during a certain period of time. This average value is used to avoid rapid switchings of

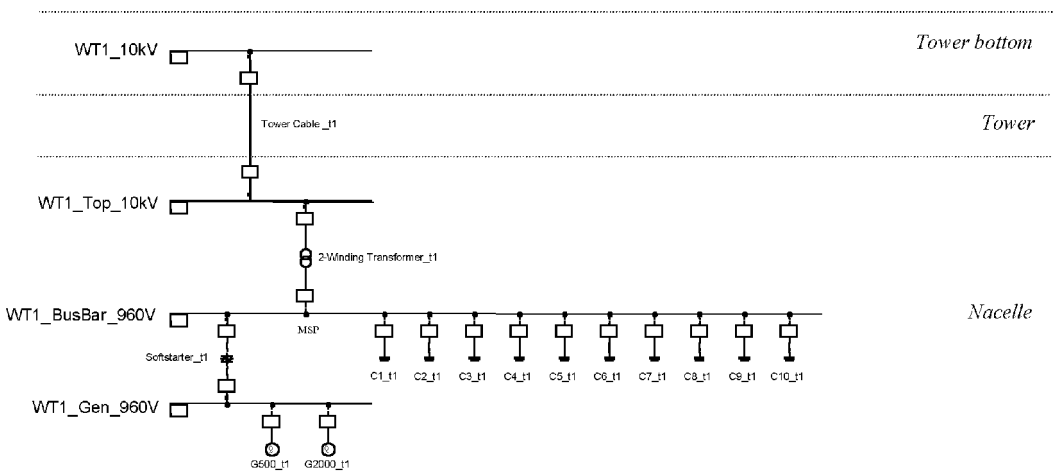

Figure 7 Single line diagram of the electrical model of the wind turbine, implemented in DIgSILENT

the capacitors, due to the short variations in the reactive power, and thus, to stabilise the switching and to protect the contacts. First a moving average of the reactive power is applied, and then a sample-hold function is used to represent block averages. The sample-hold function stores its sampled input signal at the output until the next rising edge of the clock signal appears. Such output average includes the closed loop effect of the reactive power supply from capacitors, which are already connected at a certain moment. It is then used to determine how many additional capacitors should be connected or disconnected. The total (open loop) number of capacitors, which are connected at each step, is obtained by a digital integrator, implemented in the block "Sum slot", Figure 8. At each time step, this block has information about the closed loop reactive power and the memorised number of capacitors used previously. The output of the digital integrator is then sent to the control block "Switching Slot", which opens and closes the connections of the capacitors.

5 WIND MODELLING

5.1 Introduction

A wind farm connected to the electrical grid affects the supplied power quality, due to the fluctuating character of its output power. The fluctuations are a consequence of the variations of the wind and they influence the control characteristics of the wind farm. Therefore, modelling the wind is essential in order obtain realistic simulations of the power fluctuations during continuous operation of the wind farm.

The wind model used in this article is described in detail in (Sørensen P. et al., 2001b). The emphasis here is laid on the structure and implementation issues of the model. The main advantages of this wind model are the fast computation, reduced memory requirements and the ease of use, either for variable or constant speed models. This wind speed model is very suitable for simultaneous simulation of a large number of wind turbines, making it possible to estimate efficiently the impact of a large wind farm on the power quality.

The wind model of each wind turbine combines two types of effects, namely deterministic effects and stochastic effects. The deterministic part of the wind model contains the mean wind speed and tower shadow variations. The stochastic part of the wind model includes the park scale coherence[1] between the wind turbines in a wind farm as well as the effects of the

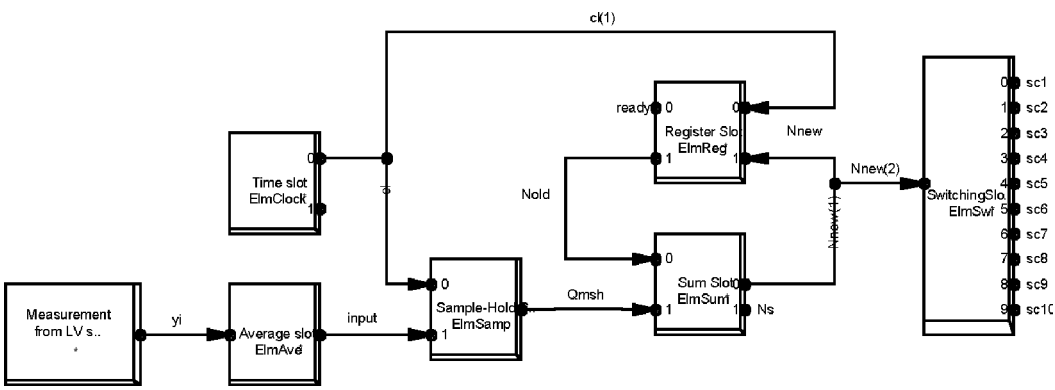

Figure 8 DIgSILENT block diagram for capacitor bank controller

1 The wind farm power production can be classified in two scale effects. The first scale depends on each wind turbine dynamics and the second scale depends mainly on the interactions between wind turbines in the park as well as the coherence of the turbulence. The turbulence between two positions is correlated. The degree of correlation depends on the distance between the two positions, the orientation of the wind and the turbulence intensity.

rotational turbulence, namely that turbulence seen by the rotating wind turbine blades. Only the horizontal component of the wind speed is considered in the model, as this component has the most dominating influence on the aero loads on wind turbine. The park scale coherence ensures more accurate predictions of the maximum output power from the wind farm, especially in the case when the wind turbines are sited very close together or when the wind blows in a direction close to the orientation of a line of wind turbines. Each wind turbine in the wind farm experiences its local version of the "global" wind turbine. The rotational turbulence and the tower shadow are included in the model because they cause fluctuations in the individual turbine power. For the 3-bladed turbines, this fluctuation is at three times the rotational frequency (3p), and is the main cause of flicker in the turbine power during continuous operation (Sørensen P., 1995). The tower shadow is modelled as a 3p fluctuation with constant amplitude, whereas the rotational sampled turbulence is modelled as a 3p fluctuation with variable amplitude (Sørensen P. et al., 2000).

The structure of the wind model is illustrated in Figure 9. It is built as a two-step model. The first step is the park scale wind model, which simulates the fixed point (hub height) wind speed $v_{hub,i}$ at each wind turbine, taking into account the park scale coherence. The second step is the rotor wind model, which for each wind turbine i, provides an equivalent wind speed $v_{eq,i}$ to the aerodynamic model – see Figure 2. The park scale model provides wind speed time series at each wind turbine hub $v_{hub,i}$ for the rotor wind model. The rotor wind models add the effect of the integration of the fixed-point fixed speed $v_{hub,i}$ over the whole rotor, the effect of the rotational turbulence and the effect of the tower shadow. The wind shear is not included in the rotor wind model, as it only has a small influence on the power fluctuations.

As illustrated in Figure 9, the wind model provides an equivalent wind speed $v_{eq,i}$ for each wind turbine i, and not an equivalent wind speed for the whole wind farm.

5.2 Park scale wind model

The park scale coherence model is a stochastic model, which simulates wind speeds with the same stochastic characteristics as measured wind speeds at fixed points. These characteristics are power spectral densities (PSDs), which describe the frequency content of

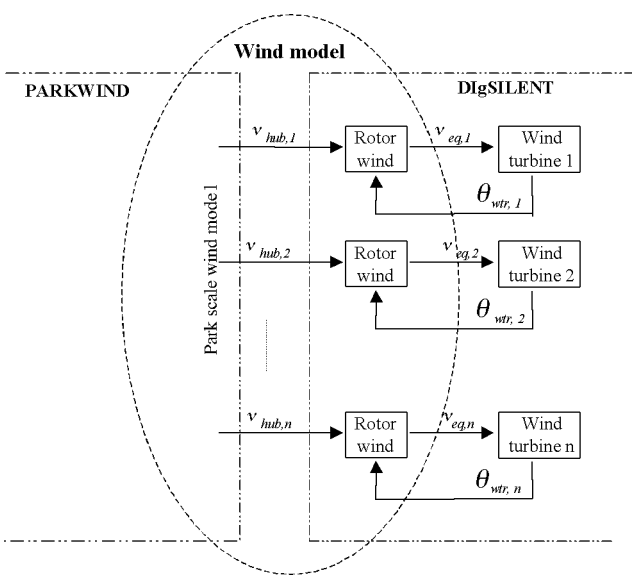

Figure 9 Simplified scheme of the wind models for a wind farm

the fluctuations, and the coherence functions, which describe the coherence between wind speeds in different points (i.e. at the wind turbines) in the frequency domain.

The park scale wind model is implemented in an external program PARKWIND, developed at Risø National Laboratory. It generates a file with wind speed time series $v_{hub,1}, \ldots v_{hub,n}$, which are then read by DIgSILENT in the rotor wind model of each wind turbine, see Figure 9. This external calculation of the hub wind speed in PARKWIND is permitted because it is assumed that the hub wind speed is independent of the wind farm operation. The hub wind speed is considered to be the wind speed at the hub height of the wind turbine, i.e. as if the wind turbine had not been erected. The present version of PARKWIND does not yet include the effects of 'wakes' in the wind farm, but modifications on the mean wind speed and turbulence intensity according to (Jensen N.O., 1983), (Frandsen S. et al., 2001) will be directly included in the next version of PARKWIND code. The PARKWIND method is capable of simulating wind speed with power spectra of either the Kaimal (Kaimal J.C. et al., 1972) or Højstrup type (Højstrup J. et al., 1990). Any coherence function is simple to use inside the PARKWIND program (Sørensen P. et al., 2001a). Davenport type coherence (Davenport A.G., 2002) and the decay factors recommended by (Schlez W. & Infield D., 1998) are used as defaults in the program.

5.3 Rotor wind model

As mentioned before, the conventional simulation program used for calculation of structural loads on wind turbines, simulates the wind speed at a large number of points in the rotor plane. Then it interpolates the wind speed between these points to provide the wind speed distribution along the blades. Finally, blade element iteration is applied to a number of sections along each blade. This is a relatively time-consuming method, and thus difficult to use for a simulation of hundreds of wind turbines.

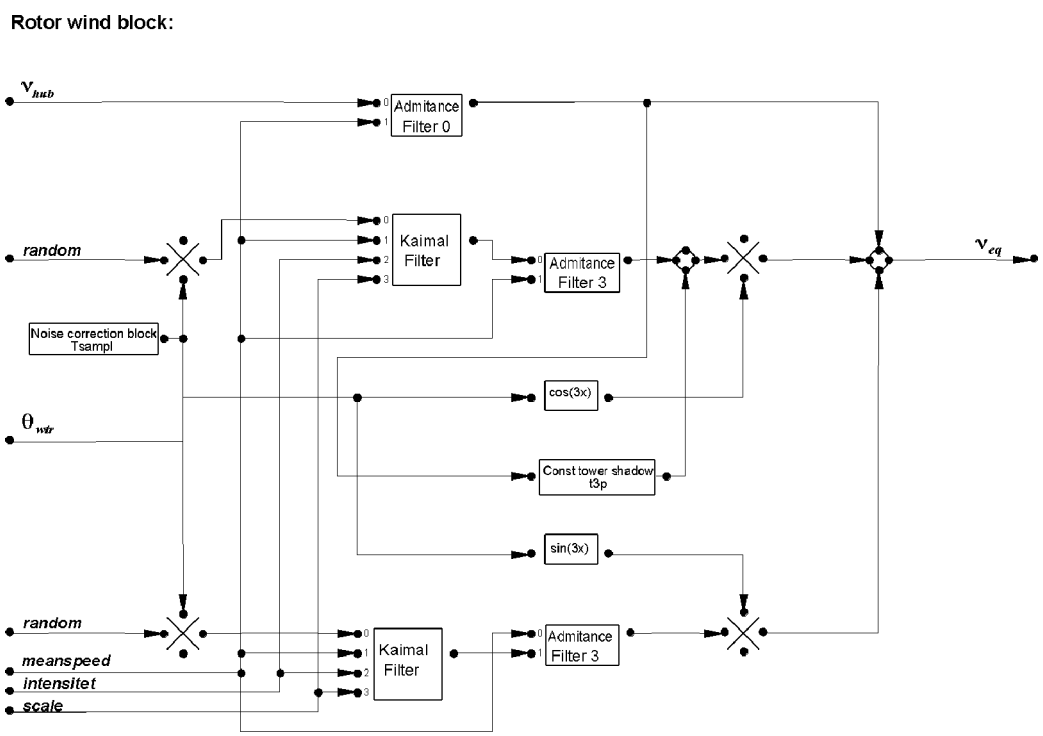

Figure 10 Rotor wind model in DIgSILENT

The idea of the rotor wind model is therefore to produce a single equivalent wind speed v_{eq} for each wind turbine, which is used as input to the aerodynamic model. Figure 10 shows the DIgSILENT implementation of the rotor wind model for each wind turbine (Sørensen P. et al., 2001a). The presence of 1p and/or 2p is an indication of some asymmetry in the 3-bladed rotor. Without loss of generality, it can be assumed that the wind turbine rotor is symmetrical and therefore the harmonics, not multiples of 3, cancel out. Therefore they are not present in the equivalent wind speed model. Furthermore, in the present implementation in DIgSILENT, it is assumed that the wind turbine structure acts like a low pass filter. This reduces the significance of the harmonics higher than 3p. Thus, the rotor wind model contains, in the first place, only the effects of zero and third order harmonics.

In the rotor wind model, the hub wind speed v_{hub} is averaged over the whole rotor (through the second order filter for zero harmonic – "Admittance Filter 0"). The variations due to the rotational turbulence and tower shadow in the wind speed field over the rotor disk are taken into account through a Kaimal filter and an admittance filter for the third harmonic – "Kaimal Filter" and "Admittance Filter 3". The Kaimal and Admittance filters fitted by (Langreder, 1996) are used.

The azimuth position of the turbine rotor θ_{wtr}, used as input in the rotor wind model, provides information about the rotational sampling, which causes fluctuations in power with three times the rotational frequency. The tower shadow is modelled as cosines with constant amplitude and phase.

6 VALIDATION AND VERIFICATION OF THE MODEL

The validation of the developed model in DIgSILENT is performed for fault free operation and it is based on power quality measurements for one of the wind turbines, assessed according to (IEC 61400-21, 2001). In this paper, the model verification focuses on the power fluctuations and the mechanical loads. Some other verification results, demonstrating the ability of the model to predict the power quality of the wind turbines, are illustrated in (Hansen A.D. et al., 2001) and in (Sørensen P. et al., 2001a).

Figure 11 shows the simulation result from DIgSILENT, for one wind turbine, at an average wind speed of 9 m/s and a turbulence intensity of 12%. As expected, the variations in the wind are transposed within the electrical power. Both the simulated equivalent wind speed and the electrical power fluctuate with three times the rotational frequency (3p).

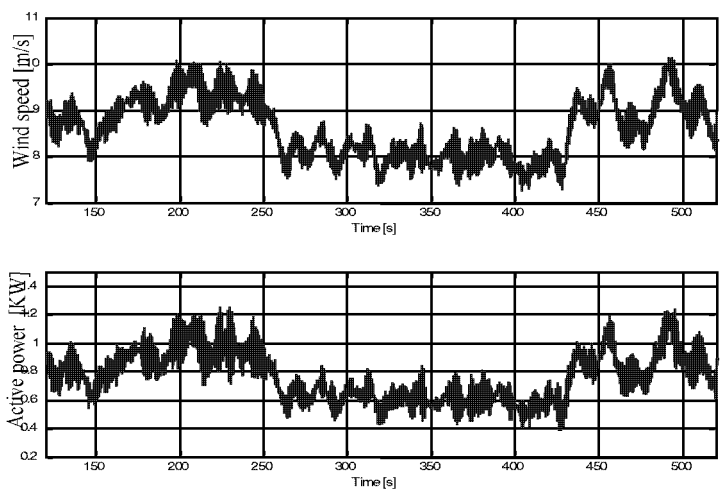

Figure 11 Simulated equivalent wind speed and simulated electrical power

As both measurements and simulation results are stochastic processes, an appropriate way to compare them is to perform a power spectral analysis. Figure 12 illustrates the power spectral density (PSD) of the measured and simulated power during continuous operation for the typical 9 m/s run. Comparing the simulated PSD to the measured one, it is observed that the low frequencies (below around 0.2 Hz) and the area around 3p frequency (0.9 Hz) are predicted quite well by the simulations.

As only the effects of zero and third harmonic for turbulence and the third harmonic from tower shadow are considered in the wind model, the 1p frequency (0.3 Hz) is not included in the model. It is only observed in the measurements and relates to some asymmetry in the rotor.

Figure 13 shows the PSD for the simulated and measured torques for the same run as in Figure 12. Two simulated torques are shown, namely the aerodynamic torque T_{ae} and the low speed torque T_{lss} (see Figure 5), together with the measured low speed torque. It is seen that the torsional vibration mode (flexibility) of the main shaft, with the eigenfrequency 0.7 Hz, provides an additional energy of T_{lss} relative to T_{ae}; i.e. the PSD of T_{lss} comes closer to the PSD of the measured torque than the PSD of T_{ae}. This indicates that the mechanical model predicts the shaft flexibility quite well. A significant 1p frequency is also present in the PSD of the measured torque. Besides the asymmetry reason of the rotor, mentioned before, in the case of the measured torque, a further reason could be that the torque measurements from strain gauges are very sensitive to 'cross talk' from shaft bending.

There are some common remarks regarding both Figure 12 and Figure 13:

- There is slightly more 3p effect in the simulated power/torque than in the measured power/torque, respectively. The spike at the 3p frequency in the simulated power and torque could indicate that the modelled tower effect is overestimated. Another factor is that the result is very sensitive to the value of the torsional eigenfrequency in the simulation, which is fairly close to the 3p frequency.
- The harmonics of higher orders than 3p, i.e. 6p (1.8 Hz), 9p (2.7 Hz) and 12p (3.6 Hz), visible in measurements, are not included in the model in the first place, since they

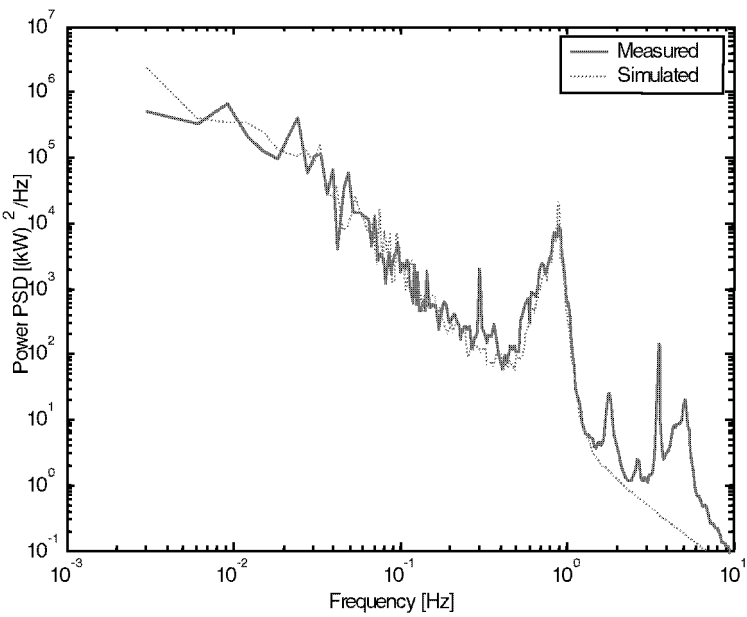

Figure 12 Power spectral density (PSD) of measured and simulated power fluctuations of wind turbine no. 1 at wind speed 9 m/s

are considered to have less influence on the power and since they increase the simulation time. However, they can be easily included in the model, if this is desired.

- There exists a significant energy around 5 Hz in the measurements, but not in the simulation. A study of measured mechanical load indicates that this frequency could be due to some kind of mechanical vibration mode of the rotor together with the tower (Sørensen P. et al., 2001a).
- The torsional vibration mode of the main shaft, with an eigenfrequency around 0.7 Hz, can be observed both in measurements and simulations.

In order to illustrate the influence of the dynamic stall effect over the whole wind speed range, a simulation of a single wind turbine is performed. In this example, the equivalent wind speed is designed (not modelled by the rotor wind model) to have a sinusoidal variation with a 3p frequency, amplitude of 2m/s and a linear increasing mean value, as it is illustrated in Figure 14. The simulation is performed with a constant pitch angle, which corresponds to 2 MW power at high wind speeds.

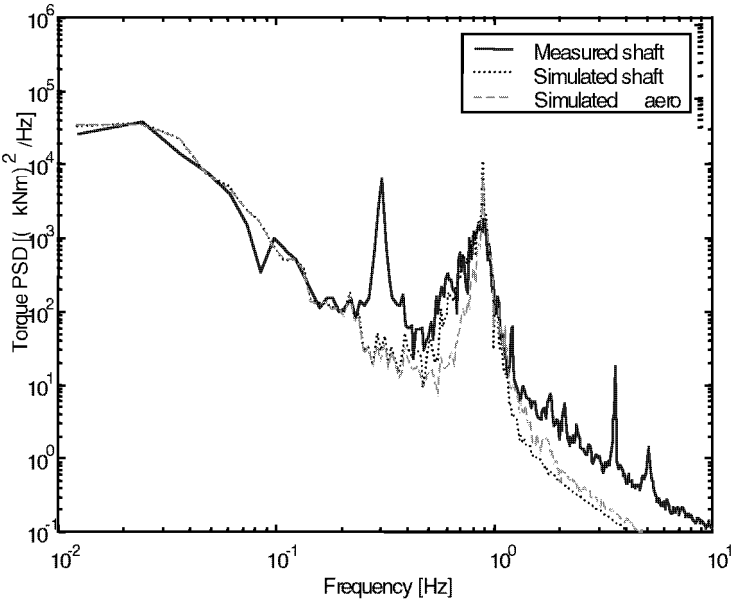

Figure 13 Power spectral density (PSD) of measured and simulated torque fluctuations of wind turbine no. 1 at mean wind speed 9 m/s

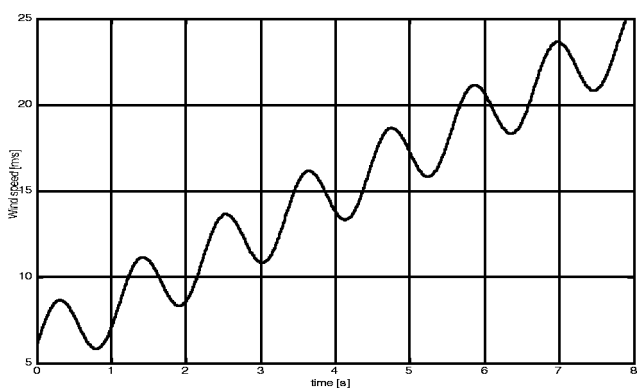

Figure 14 Designed equivalent wind speed – input for wind turbine simulation

Figure 15 shows the profile of the dynamic power curve, modelled with and without dynamic stall. The cyclic behaviour of the sinusoidal wind speed input signal is transferred through the second order dynamic model of the transmission system to other signals, such as the aerodynamic power, the aerodynamic torque and the rotor speed ω with a corresponding phase shift. The significantly increased amplitude of the dynamic power fluctuations at high wind speeds illustrates that the dynamic stall effect is important at large wind speeds, while at small wind speeds it is not relevant. The improved aerodynamic model with the dynamic effect is thus able to simulate the larger fluctuations in the power in the stall region. It is also observed that even the power curve without dynamic stall has some cyclic behaviour. This is due to the sinusoidal wind speed input signal, which is transferred to the other state variables through the model dynamics. Beside the sinusoidal wind speed, the aerodynamic efficiency without dynamic stall, expressed as a function of wind speed, $C_p(v,\theta)$, also influences the calculation of the small cycles in the power curve without dynamic stall.

Figure 16 illustrates the aerodynamic efficiency as a function of tip speed ratio, $\lambda=\omega R/v$, for the steady state, attached, separated and dynamic flow, in the conditions of the previous simulation. It is observed that the steady state aerodynamic efficiency, C_p^{static}, illustrated this time as function of λ, does not contain any cycles. This is because C_p^{static} is an algebraic function of rotor speed ω, wind speed v and pitch angle θ. It is also noted that the steady state C_p^{static} converges to the attached $C_p^{attached}$ aerodynamic efficiency at high λ values (low wind speeds), while at small λ values (large wind speeds), the steady state C_p^{static} converges to the separated $C_p^{separated}$. Moreover, at small wind speeds, the steady state C_p^{static} aerodynamic efficiency and the dynamic aerodynamic efficiency $C_p^{dynamic}$ do not differ significantly, because at small wind speeds the dynamic stall effect is not relevant. At large wind speeds (small λ values) the values of the dynamic aerodynamic efficiency $C_p^{dynamic}$ are retarded with the time constant τ of the first order filter (see Figure 4), and then move toward the steady state aerodynamic efficiency C_p^{static} on an almost "parallel" curve with the attached and separated efficiency curves. The calculated value of $C_p^{dynamic}$ is interpolated between these "parallel" curves, which correspond to different separation ratios f (Sørensen P. et al., 2001a). The dynamic value $C_p^{dynamic}$ is the result of the first order filter, which physically corresponds to the fact that, it remains for a time lag on a specific intermediary curve. Thus, at large wind speeds, the variation of $C_p^{dynamic}$ is different from that of C_p^{static}.

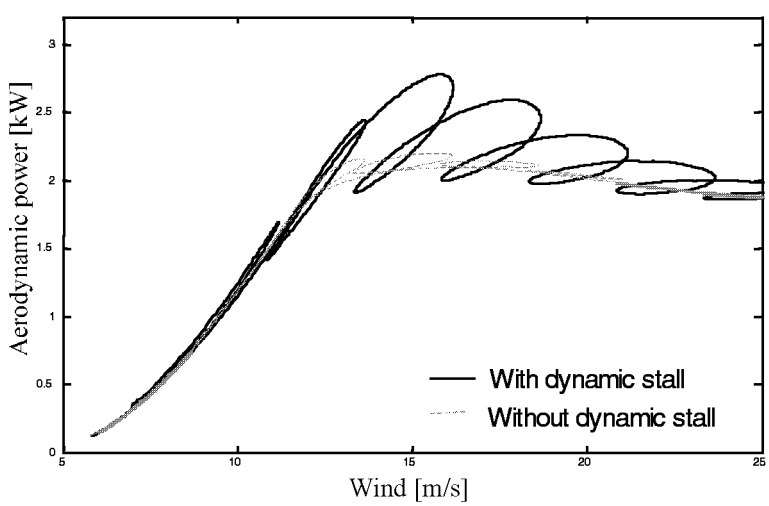

Figure 15 Power curve with and without dynamic stall effect

Figure 17 illustrates the PSD analysis for both measured and simulated power fluctuations at a large mean wind speed of 14 m/s. Two simulations are performed, one with and one without the dynamic stall model. It is observed that the dynamic stall model improves the simulations slightly, even though the PSD of the simulation without the dynamic stall model looks acceptable.

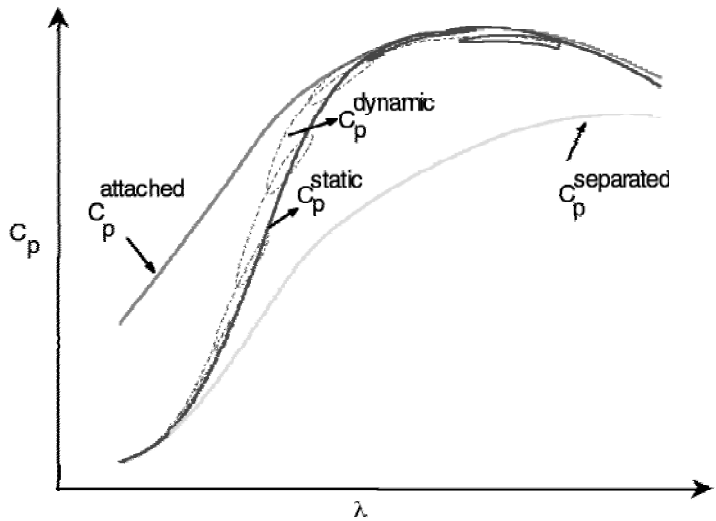

Figure 16 Steady state, attached, separated and dynamic aerodynamic efficiency as a function of λ

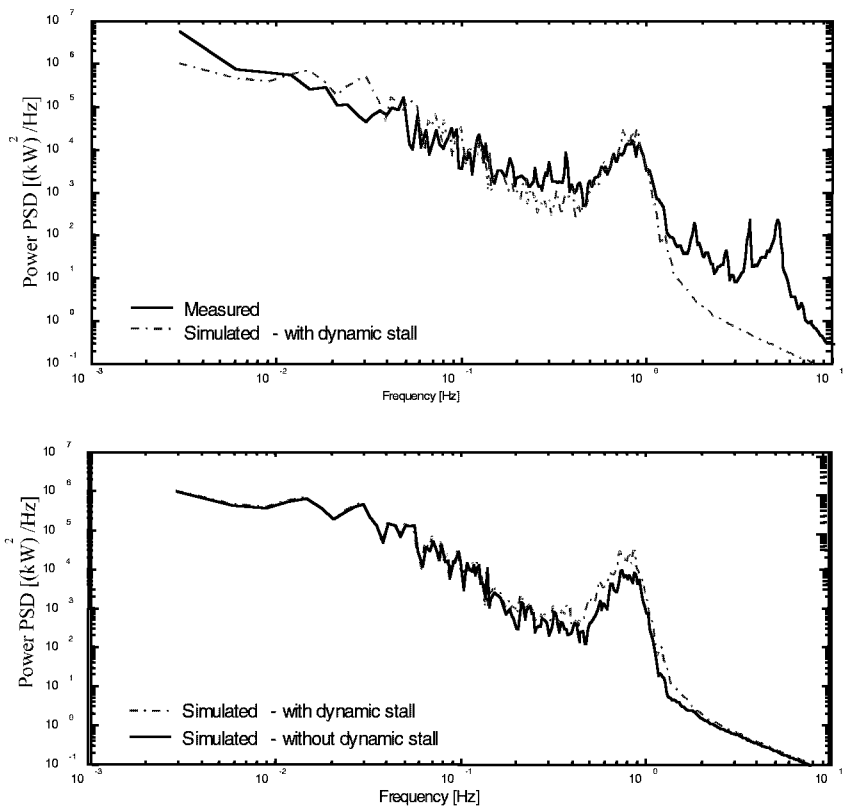

Figure 17 PSD of measured and simulated power fluctuations of wind turbine no. 1 at wind speed 14 m/s

However, a more detailed impression on the character of the fluctuations is achieved on the time series, illustrated in Figure 18. Two simulations are done with identical wind speed input. It should be noticed that the simulated and the measured time series do not have the same wind speed time series, so they cannot be compared step by step. The idea of the comparison with the measured time series is just to show how large the power fluctuations are in reality, as compared to those simulated. The character of the first 300 seconds of the simulations is in good agreement with the measurements (the simulations have a slow variation), while the character in the last 300 seconds of simulations is significantly different. Here the simulations have very reduced slow fluctuation. The fast (3p) fluctuations in the simulation without dynamic stall are also strongly reduced due to the flat character of the power curve in the stall region, as the wind speed increases (see Figure 3). On the other hand, the dynamic stall model improves the simulation of the fast fluctuations in the stall region.

However, it is noticed that the slow fluctuations are not simulated well enough. There are two possible reasons for this. One reason can be that the wind model only includes the horizontal component of the wind speed. The transverse wind speed component is quite important in the region of large wind speeds as compared to the region of small wind speeds, due to: (1) the power fluctuations are much larger at increased wind speeds, (2) the efficiency curve $C_p(\lambda, \theta_{pitch})$ is very steep in that region. Studies of the slope of the efficiency curve in the stall region have shown that a transverse component of the wind speed of 1 m/s will increase C_p by 5%, corresponding to in this case to 100 kW (Sørensen P. et al., 2001a). Another reason for the absence of slow fluctuations in the simulations may be the uncertainty of the aerodynamic data.

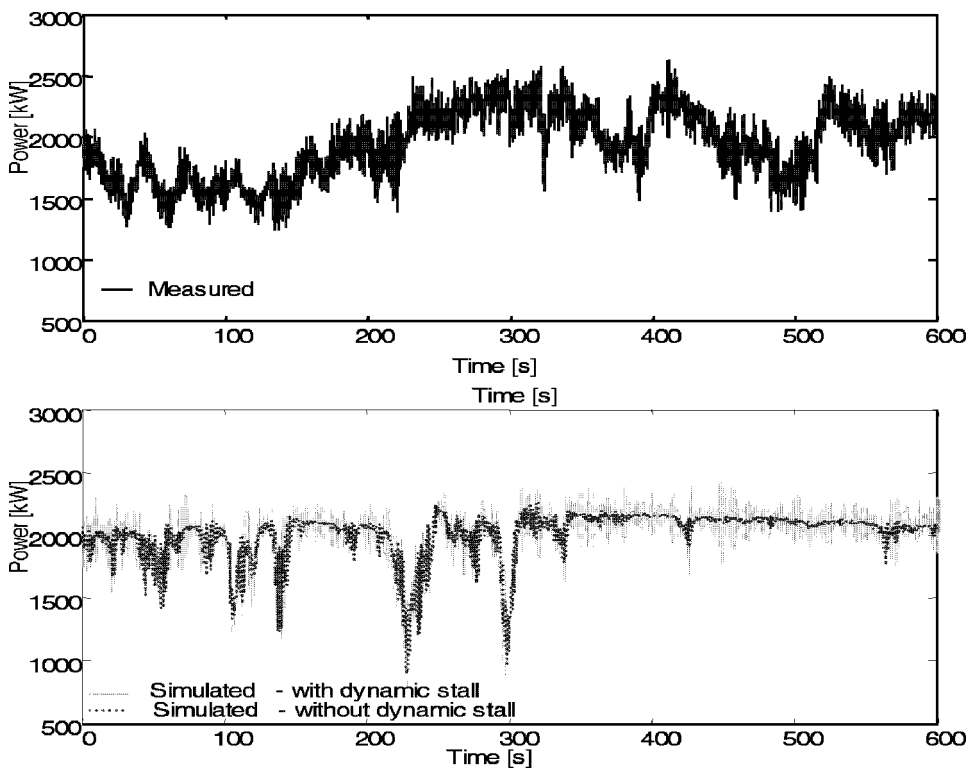

Figure 18 Time series of measured and simulated power fluctuations of wind speed 14 m/s

7 CONCLUSIONS

The present work provides a wind farm dynamic model, as a first step towards the long-term objective of developing tools for study and improvement of the dynamic interaction between wind farms and power systems to which they are connected.

The whole wind farm dynamic model, which includes the main effects that contribute to the fluctuation of the power from a wind farm, has been developed and implemented in the power system simulation tool DIgSILENT. It comprises the substation where the wind farm is connected, the internal power collection system of the wind farm, the wind dynamics and the wind turbines. The individual wind turbine model contains the mechanical model, the aerodynamic model (improved with a model for dynamic stall effects) and the electrical model (with submodels for induction generator, soft-starter, capacitor bank for reactive power compensation and transformer).

The implemented wind farm model can be easily extended to model other large wind farms, with other wind turbines. It is built to enable assessment of power quality and control strategies. The model has been validated for fault-free operation. The verification, based on one wind turbine, shows generally good agreement between simulations and measurements, although the simulations at larger wind speeds seem to underestimate the power fluctuations. Agreement can be improved by including the transverse component of the wind speed in the model. The implemented model is able to simulate a whole wind farm with respect to the electrical power. The next steps are to enhance the model to predict the behaviour of the wind farm in the event of grid faults and to benchmark the model on data from a wind farm connected to a transmission network.

8 ACKNOWLEDGEMENT

This work was carried out by the Wind Energy Department at Risø National Laboratory in co-operation with Aalborg University and NEG-Micon Control Systems. The authors acknowledge the financial support to the project by the Danish Energy Agency contract #1363/00-0003. The co-operation with NegMicon Control System A/S has also been very useful. Special thanks are given to the North-West Sealand Energy Supply Company, NVE, which provided grid data and assisted in the power quality measurements.

REFERENCES

Davenport A.G. (1961). *The spectrum of horizontal gustiness near the ground in high winds*. Q.J.R.Meteorol.Soc., 87, 194–211.

DEFU (1998). *Connection of wind turbines to low and medium voltage networks.*, Report no. KR111-E, Elteknikkomiteen (1998-10-09).

Eltra (2000). *Specifications for Connecting Wind Farms to the Transmission Network*. ELT 1999-411a, Eltra, http://www.eltra.dk.

Frandsen S., Thøgersen, & M.L. (2001). *Integrated fatigue loading for wind turbines in wind farms by combining ambient turbulence and wakes*. Wind Engineering, vol. 23, pp. 327–340.

Hansen A.D., Sørensen P., Janosi L., & Bech J. (2001). *Wind farm modelling for power quality*. Proc. IECON '01, held in Denver, USA ..

Højstrup J., Larsen S.E., & Madsen P.H. (1990). *Power spectra of horizontal wind components in the neutral atmospheric boundary layer*. In Ninth Symposium of Turbulence and Diffusion, ed. N.O. Jensen, L. Kristiansen and S.E. Larsen.American Meteorology Society, pp. 305–308.

IEC 61400-21 (2001). *Wind turbine generator systems – Part 21: Measurement and assessment of power quality characteristics of grid connected wind turbines*. Final Draft International Standard 88/ 144/ FDIS International Electrotechnical Commission, IEC 2001-07-01, Ed.1.

Jensen N.O. (1983). *A note on wind generator interaction*. Risø National Laboratory, Roskilde, Denmark. Risø–M-2411.

Kaimal J.C., Wyngaard J.C., Izumi Y., & Cote O.R. (1972). *Spectral characteristics of surface layer turbulence*. Q.J.R.Meteorol.Soc., 98, pp 563–598.

Langreder,W. (1996). *Models for variable speed wind turbines*. M.Sc. Thesis, Crest Loughborough University and Risø National Laboratory.

Schlez W., & Infield D. (1998). *Horizontal, two point coherence for separations greater than the measurement height*. Boundary-Layer Meteorology 87. Kuvwer Academic Publishers, Netherlands, pp.459–480.

Sørensen P. (1995). *Methods for calculation of the flicker contribution from wind turbines*. Risø National Laboratory, Roskilde, Denmark. Risø-I-939.

Sørensen P., Hansen A.D., Janosi L., Bech J., & Bak-Jensen B. (2001a). *Simulation of interaction between wind farm and power system*. Risø National Laboratory. Risø-R-1281.

Sørensen P., Hansen A.D., & Rosas P.A.C. (2001b). *Wind models for prediction of power fluctuations from wind farms*. Proc 'The Fifth Asia-Pacific Conference on Wind Engineering (APCWEV)', Kyoto, Japan. Journal of Wind Engineering no.89, pp. 9–18.

Sørensen P., Bak-Jensen B., Kristiasen J., Hansen A.D., Janosi L., & Bech J. (2000). *Power plant characteristics of wind farms*. Wind Power for the 21st Century. Proceedings of the International Conference held at Kassel, Germany 25–27 September.

Øye,& S. (1991). *Dynamic stall – simulated as time lag of separation*. Proceedings of the 4th IEA Symposium on the Aerodynamics of Wind Turbines. McAnulty, K.F. (Ed.), Rome, Italy.